Limiting radiation damage for high-brilliance biological solution scattering: practical experience at the EMBL P12 beamline PETRAIII

Cy M. Jeffries, Melissa A. Graewert, Dmitri I. Svergun and Clément E. Blanchet

Synchrotron radiation research is rapidly expanding with many new sources of radiation being created globally. Synchrotron radiation plays a leading role in pure science and in emerging technologies. The *Journal of Synchrotron Radiation* provides comprehensive coverage of the entire field of synchrotron radiation research including instrumentation, theory, computing and scientific applications in areas such as biology, nanoscience and materials science. Rapid publication ensures an up-to-date information resource for scientists and engineers in the field.

Crystallography Journals Online is available from **journals.iucr.org**

Limiting radiation damage for high-brilliance biological solution scattering: practical experience at the EMBL P12 beamline PETRAIII

Cy M. Jeffries, Melissa A. Graewert, Dmitri I. Svergun and Clément E. Blanchet*

European Molecular Biology Laboratory Hamburg Outstation, c/o Deutsches Elektronen-Synchrotron, Notkestrasse 85, Hamburg 22603, Germany. *E-mail: clement.blanchet@embl-hamburg.de

Radiation damage is the general curse of structural biologists who use synchrotron small-angle X-ray scattering (SAXS) to investigate biological macromolecules in solution. The EMBL-P12 biological SAXS beamline located at the PETRAIII storage ring (DESY, Hamburg, Germany) caters to an extensive user community who integrate SAXS into their diverse structural biology programs. The high brilliance of the beamline [5.1×10^{12} photons s^{-1}, 10 keV, 500 (H) μm $\times$ 250 (V) μm beam size at the sample position], combined with automated sample handling and data acquisition protocols, enable the high-throughput structural characterization of macromolecules in solution. However, considering the often-significant resources users invest to prepare samples, it is crucial that simple and effective protocols are in place to limit the effects of radiation damage once it has been detected. Here various practical approaches are evaluated that users can implement to limit radiation damage at the P12 beamline to maximize the chances of collecting quality data from radiation sensitive samples.

Keywords: protein; radiation damage; synchrotron small-angle scattering; SAXS.

1. Introduction

The advantages afforded by synchrotron beamlines for biological small-angle X-ray scattering (SAXS) investigations, that include small-sample volumes and rapid data acquisition (Franke *et al.*, 2012; Grant *et al.*, 2011; Hura *et al.*, 2009; Nielsen *et al.*, 2012; Blanchet *et al.*, 2012; Martel *et al.*, 2012), can be rendered ineffective if samples undergo radiation damage. For dilute protein samples, radiation damage manifests itself as irreversible aggregation, unfolding or fragmentation (Kuwamoto *et al.*, 2004; Fischetti *et al.*, 2003). At the energies (5–15 keV) and X-ray fluxes encountered at synchrotron facilities ($>10^{11}$ photons s^{-1} with beam sizes typically <5 mm^2), free hydroxyl (OH$^\bullet$) and hydroperoxyl (HO$_2^\bullet$) radicals and solvated electrons are produced from the photolysis of water (Garrison, 1987; Maleknia *et al.*, 2001). These highly reactive species combined with free radicals formed by protein X-ray absorption (in particular for those proteins containing higher atomic mass elements, *e.g.* metalloproteins) result in very fast radical activation of the polypeptide chain (10^9–10^{10} M^{-1} s^{-1}). This activation drives the aggregation process (Kuwamoto *et al.*, 2004; Garrison, 1987). Thus, the main source of radiation damage is from the supporting aqueous solvent, which explains its frequent occurrence during solution-based biological SAXS measurements.

Strategies to reduce radiation damage include increased sample flow-rates, translating the sample cell/capillary through the beam, beam attenuation, beam defocusing and reduced exposure time (Fischetti *et al.*, 2003; Pernot *et al.*, 2010; Martel *et al.*, 2012). The addition of small molecules such as dithiothreitol (DTT) and ascorbic acid to the supporting solvent, referred to as radical scavengers, can also yield increased resistance to radiation damage (Grishaev, 2012; Jacques & Trewhella, 2010). Polyols (glycerol, ethylene glycol or sucrose), although not scavengers *per se*, influence long-range protein–protein interactions as well as irreversible association and thus are effective in reducing radiation-induced aggregation (Kuwamoto *et al.*, 2004). A rather elegant strategy to reduce radiation damage is to employ cryo-SAXS where protein samples are flash cooled into a vitrified glass using cryo-protectants (*e.g.* polyethylene glycol) and maintained in a vitrified state during data collection (Meisburger *et al.*, 2013). However, cryo-SAXS is technically cumbersome, requiring highly specialized instrument stages and significantly complicates sample preparation (*e.g.* obtaining solution conditions that always form a consistent glass while at the same time maintaining samples in a monodisperse state without compromising X-ray contrast). Each of these methods provides alternative options to curb the effects of radiation damage, yet each comes with an associated cost. For solution-SAXS these costs include reduced signal-to-noise ratios in the

data caused by beam attenuation, defocusing, or reduced contrast and potentially deleterious alterations to the sample as a result of chemical changes to the solvent (*e.g.* DTT and the reduction of disulfide bonds). For experienced SAXS practitioners and beamline scientists it can be well worth optimizing beamline and sample conditions to reduce radiation damage to as low as reasonably achievable. However, conditions are likely to change on a case-by-case basis depending on the sample, which complicates high-throughput operations at facilities with extensive user programs.

In the first full year of operation (beam-year 2013) over 180 projects were performed at the EMBL P12 BioSAXS beamline by nearly 140 groups with a total of more than 400 user-visits. The beamline has been purposely designed to cater for a diverse user community spanning novices to experts. Automated sample handling, data acquisition, processing and analysis tools enable the measurement of anywhere between 3 and 2000 samples during an experimental time slot. The two most popular instrument configurations for user operations are 'batch mode' analysis that utilizes automated sample delivery with continuous sample flow through a quartz capillary, held under vacuum, to the beamline (20×50 ms exposures for 1 s) and in-line size-exclusion chromatography SAXS, or SEC-SAXS, that performs mobile phase component separation immediately prior to the X-ray cell (1 s continuous exposures for up to 3600 frames). It is necessary to balance the detection of radiation damage with the allocated user time and deploy practical and time-efficient ways to limit this damage during the course of an experiment. The data-processing software pipeline implemented at P12 (Franke *et al.*, 2012) has in-built statistical checks that in near real-time (1–2 s after data acquisition, in batch mode) compares data frames to identify, flag and remove data affected by radiation damage prior to further automated processing. The aim of this short communication is to evaluate what practical solutions users can implement within their allocated time at P12 to reduce radiation damage in sensitive samples. These strategies are heavily influenced, and inspired, by the work of Kuwamoto, Akiyama and Fujisawa (Kuwamoto *et al.*, 2004) who offer a detailed study of the effects of radiation damage to proteins in solution.

2. Materials and methods

2.1. Sample preparation

Glucose isomerase, GI (xylose isomerase), was purchased as a crystalline suspension from Hampton Research while bovine serum albumin (BSA), horse heart cytochrome-C and bovine pancreatic ribonuclease A (RNAse) in their powdered forms were purchased from Sigma. Chicken egg-white lysozyme, also in powdered form, was sourced from USB Corporation. These proteins are all well characterized SAXS standards (Mathew *et al.*, 2004; Mylonas & Svergun, 2007). The proteins were dissolved and dialysed overnight at 277 K against the following buffers: GI, 200 mM NaCl, 1 mM MgCl$_2$, 10 mM MES, pH 7.0; BSA, 50 mM HEPES, pH 7.5; cyto-

chrome-C and RNAse, phosphate buffered saline, pH 7.0; and lysozyme, 150 mM NaCl, 40 mM sodium acetate, pH 3.8. The final sample concentrations were determined using the appropriate extinction coefficients at 280 nm, expressed as $E_{0.1\%}$ (mg ml^{-1}), calculated from the primary amino acid sequence (ProtParam; Gasteiger *et al.*, 2005) except for cytochrome-C where the concentration was estimated based on the dry weight used to make up the sample. The Abs$_{280nm}$ $E_{0.1\%}$ of each sample were: GI, 1.074 mg ml^{-1}; BSA, 0.614 mg ml^{-1}; RNAse, 0.653 mg ml^{-1}; lysozyme, 2.653 mg ml^{-1}. The final concentrations used are reported in the results. Three solution additives were tested for their effects on limiting radiation damage during X-ray exposure: dithiothreitol (DTT), ascorbic acid and glycerol. These additives were made up as fresh $10\times$ concentrated stock solutions in the respective post-dialysis buffers (DTT, 10 mM; ascorbate, 10 mM; glycerol, 50% v/v) and pH adjusted accordingly to prevent pH shock when diluted into the protein samples. The final concentrations of each additive used for the radiation damage experiments were 1 mM DTT, 1 mM ascorbate and 5% v/v glycerol.

2.2. SAXS data collection

The SAXS intensity data [$I(q)$ *versus* q, where $q = 4\pi \sin\theta/\lambda$, 2θ is the scattering angle] were acquired at a photon flux of 5.1×10^{12} photons s^{-1} at 10 keV ($\lambda = 0.124$ nm) using a three-pair slit collimated incident beam with a maximum dimension of 500 (H) μm $\times$ 250 (V) μm at the sample position [200 (H) μm $\times$ 110 (V) μm, FWHM]. Samples were housed in a 1.8 mm quartz capillary (1.7 mm internal diameter) held at 283 K under vacuum. [In agreement with Kuwamoto *et al.* (2004), higher sample temperatures (283–313 K) produced only minor effects with respect to the initial rates of X-ray induced radiation damage (*i.e.* aggregation); data not shown]. Data were collected using a DECTRIS PILATUS 2M photon-counting detector with a 30 Hz frame rate and 2.2 ms readout time. A non-standard batch mode sample delivery and collection scheme was employed. Continuous-flow automated sample delivery was disabled and replaced with manual loading (10 μl) with static sample data collection. Data from lysozyme were collected with or without different levels of beam attenuation using different exposure times ranging from 50 ms to 1.41 s, over 20–100 successive data frames. Beam attenuation to 7.3×10^{11} photons s^{-1} (medium attenuation) or 1.8×10^{11} photons s^{-1} (high attenuation) was achieved by moving 300 μm- or 480 μm-thick aluminium foils into the incident beam path. Solution additive experiments (DTT, ascorbate and glycerol) were performed on GI, BSA, cytochrome-C, RNAse and lysozyme using the full unattenuated beam. Details of the exact exposure times and attenuation factors are reported in the results.

2.3. SAXS data analysis

Qualitative measures of the effects of radiation damage to each protein sample were evaluated using a Guinier approximation based on $I(q) = I(0) \exp(-R_g^2 q^2/3)$, where R_g is the

radius of gyration and $I(0)$ the total forward scattering recorded at zero angle (Guinier, 1939). In typical instances (*e.g.* for a globular protein in solution) the linear extrapolation of $\ln[I(q)]$ *versus* q^2 at low angle calculated at $qR_g < 1.3$ should provide both the magnitude of $I(0)$ at the $q = 0$ intercept and a linear slope that relates to the R_g of the particle. Each of the proteins investigated in this study adhere to the Guinier approximation as monodisperse samples and the R_g value for each protein is known in the undamaged state (Mylonas & Svergun, 2007; Graceffa *et al.*, 2013; Mathew *et al.*, 2004). Consequently, the R_g values from undamaged samples can be used as a frame of reference in which to monitor the effects of radiation exposure even though the linear relationship in the Guinier plot breaks down as a result of accumulating aggregates. The sensitivity of R_g to the shape and size of particles in solution (a 0.1 nm increase in R_g of a globular protein represents significant mass redistribution) makes R_g a simple and convenient probe to quantify damage. Therefore, a forced linear regression of $\ln[I(q)]$ *versus* q^2 across a fixed qR_g range corresponding to $0.8 < qR_g^u < 1.3$ was used as an empirical measure of radiation damage, where R_g^u is the radius of gyration of the undamaged proteins. The slopes of the linear fits to the data were used to calculate pseudo-R_g values (R_g^{ps}) for the damaged samples. It must be emphasized that the pseudo-R_g values using this approach do not correspond to the actual R_g of the aggregated samples, but are only used to characterize the accumulation of aggregates, specifically in terms of 'initial rates of damage' that we define as ΔR_g^{ps} s^{-1} which were calculated from the first five frames of each dataset and normalized to unit time. The similarity between data frames was assessed using the reduced χ^2 test implemented in the DATCMP tool of the *ATSAS* package (Petoukhov *et al.*, 2007, 2012). The significance level is set at 0.01, *i.e.* when comparing frames, $p > 0.01$ indicates similarity.

2.4. Calculation of critical dose

The critical dose, D, in Gy, or the energy per kg (J kg^{-1}) required to change R_g^{ps} by a maximum of 0.1 nm relative to the initial data frame, was calculated using a relationship derived from Meisburger *et al.* (2013) taking into account the finite path length of the sample:

$$D = 1000 \ \frac{Etf}{\rho_m A L} \left[1 - \frac{1}{\exp(\mu \rho_m L / \rho)} \right], \qquad (1)$$

where E is the energy per photon (in J photon^{-1}). The value t, the critical dose time (in s), was derived either directly from plots of R_g^{ps} *versus* time (see Fig. S1 of the supporting information[1]) or from extrapolated times calculated from the initial rate estimates (ΔR_g^{ps} s^{-1}). Here, f represents the beam flux (photons s^{-1}) experienced by the sample, taking into account the transmission of the first 50 μm quartz wall of the capillary (assuming the mass density of quartz to be 2.648 g cm^{-3}). The quartz transmission was calculated using the Center for X-ray Optics server (http://henke.lbl.gov/optical_constants/

---

[1] Supporting information for this paper is available from the IUCr electronic archives (Reference: XH5041).

filter2.html; Henke *et al.*, 1993). The mass density of the sample, ρ_m (g cm^{-3}), was calculated using *MULCh* (Whitten *et al.*, 2008), while A (cm^2) is the total beam area and L (cm) the thickness of the sample (corresponding to the internal capillary diameter of 0.17 cm). The average mass attenuation coefficient, μ/ρ (cm^2 g^{-1}), of each sample, without coherent scattering, was calculated from the total atomic composition using the XCOM Photon Cross Sections Database (http://www.nist.gov/pml/data/xcom/index.cfm; Berger *et al.*, 2010). The atomic formulae of each protein were calculated using ProtParam (Gasteiger *et al.*, 2005). The factor 1000 converts J g^{-1} into J kg^{-1} to obtain Gy. Note that the above relationship calculates the dose delivered to the sample averaged across the maximum beam size (0.00125 cm^2), *i.e.* it assumes an average homogeneous illumination through the total beam area, as opposed to calculating the dose at the peak of the beam intensity (0.00022 cm^2 FWHM). For further information, including the values of μ/ρ, refer to Tables S1–S4 of the supporting information.

3. Results and discussion

3.1. Flow-enabled *versus* static sample data collection

Fig. 1(*a*) displays SAXS data measured from a lysozyme sample (4 mg ml^{-1}; 5 × 50 ms frames) using the default user collection scheme of the P12 beamline, *i.e.* with sample flow enabled (30 μl s^{-1}) under full-beam intensity (5.1 × 10^{12} photons s^{-1}, 10 keV). Data are plotted on a log–log scale to emphasize the low-*s* regions of the scattering data where any effect caused by damage becomes manifest in the scattering intensities. In this instance, the five data frame overlay and the scattering profiles appear 'flat' at low-*q*, suggesting that radiation damage is negligible. When comparing data frames, subtle radiation damage can be identified at very low angles after 250 ms exposure (frame 1 *versus* frame 5, $p = 0.006$). Consequently, even with sample flow enabled, radiation damage to samples can still occur. However, the initial rate of change in R_g^{ps} of lysozyme (ΔR_g^{ps} s^{-1}) as shown in Fig. 1(*c*) (∼0–0.1 nm s^{-1}) supports the case that sample flow significantly reduces damage in contrast to using a static sample data collection strategy (Fig. 1*b*). When the sample flow is stopped, systematic increases in the scattering intensity at low angle are observed with increasing time in the successive data frames. The initial ΔR_g^{ps} s^{-1} increases to 5.5 nm s^{-1} [Fig. 1(*c*), black diamonds] and after 50 ms exposure the sample is damaged. For the results reported in the remainder of this study, data were collected with disabled flow, *i.e.* using a non-standard data collection protocol. This choice was deliberate: first, it facilitated controlled radiation delivery to the same volume of sample for subsequent comparative analyses and, second, it generated more extreme radiation environments than that which user samples typically experience.

3.2. Beam attenuation

Beam attenuation at the P12 beamline is straightforward and is performed by a single button click on a GUI that allows

Cy M. Jeffries *et al.* · Limiting radiation damage for biological solution scattering **275**
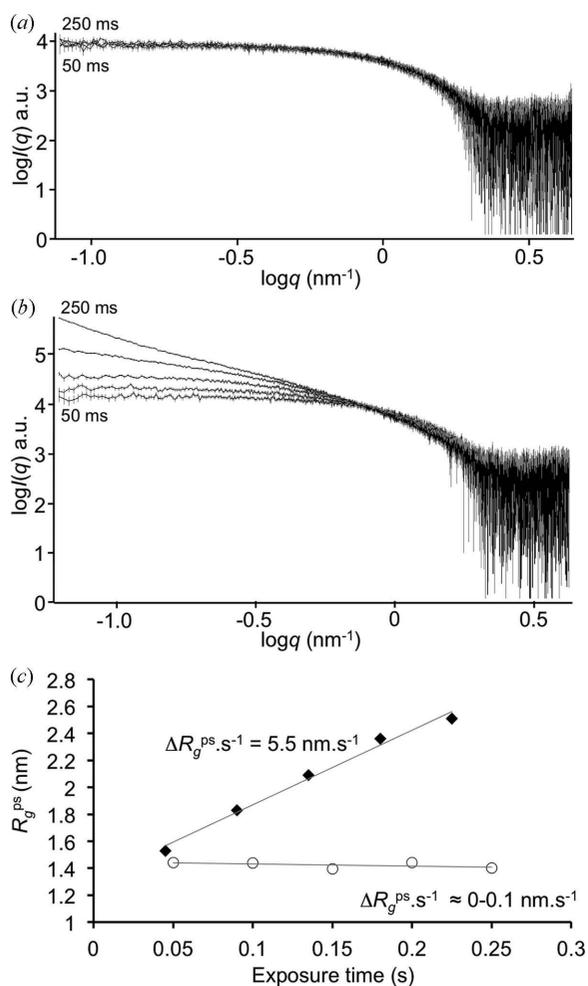
Figure 1
The effects of sample flow on radiation damage to lysozyme samples. (a) Five lysozyme SAXS data frames collected using the default P12 beamline user collection strategy where sample flow is enabled at full beam intensity (5.1×10^{12} photons s^{-1}, 10 keV). (b) SAXS data recorded for lysozyme with the sample flow stopped. (c) The relationship between the pseudo-R_g parameter (R_g^{ps}) used to qualify initial rates of radiation damage *versus* exposure time, comparing lysozyme samples collected under 'no-flow' (black diamonds) or sample-flow conditions (open circles).

aluminium foils of different thicknesses (300 and 480 µm) to be moved into the incident beam. Figs. 2(a)–2(c) show the effects of beam attenuation on SAXS data collected from lysozyme at 4.4 mg ml^{-1} for 5 × 50 ms exposures. At full photon flux (5.1×10^{12} photons s^{-1}) damage to the sample is apparent (frame 1 *versus* frame 2, $p = 0$), and a systematic reduction in damage occurs as the flux is decreased to 7.3×10^{11} photons s^{-1} (frame 1 *versus* frame 5, $p = 0.4$) and 1.8×10^{11} photons s^{-1} (frame 1 *versus* frame 5, $p = 0.09$), respectively, as shown in Fig. 2(d). The critical absorbed dose in kGy (J kg^{-1}) of lysozyme, or the point at which ΔR_g^{ps} changes by 0.1 nm relative to the initial data frame, lies in the range 0.28–0.35 kGy for the attenuation series. These values are of a similar magnitude of 0.4 kGy reported by Kuwamoto *et al.* (2004) for lysozyme using an identical buffer at similar protein concentrations, where both approaches estimate the critical dose by monitoring the radius of gyration and formation of

aggregates. The time taken for the aggregates to form are 0.018, 0.135 and 0.45 s for no, medium and high attenuation, respectively. These times are shorter than Kuwamoto's at ∼2.1 s, reflecting differences in energy (13.8 keV), flux (2.2×10^{11} photons s^{-1}) and, importantly, the larger beam area [800 (H) µm × 600 (V) µm] used for the experiment. Consequently, the critical dose values reported here (see Table S4) need to be interpreted with caution: at a practical level, it is
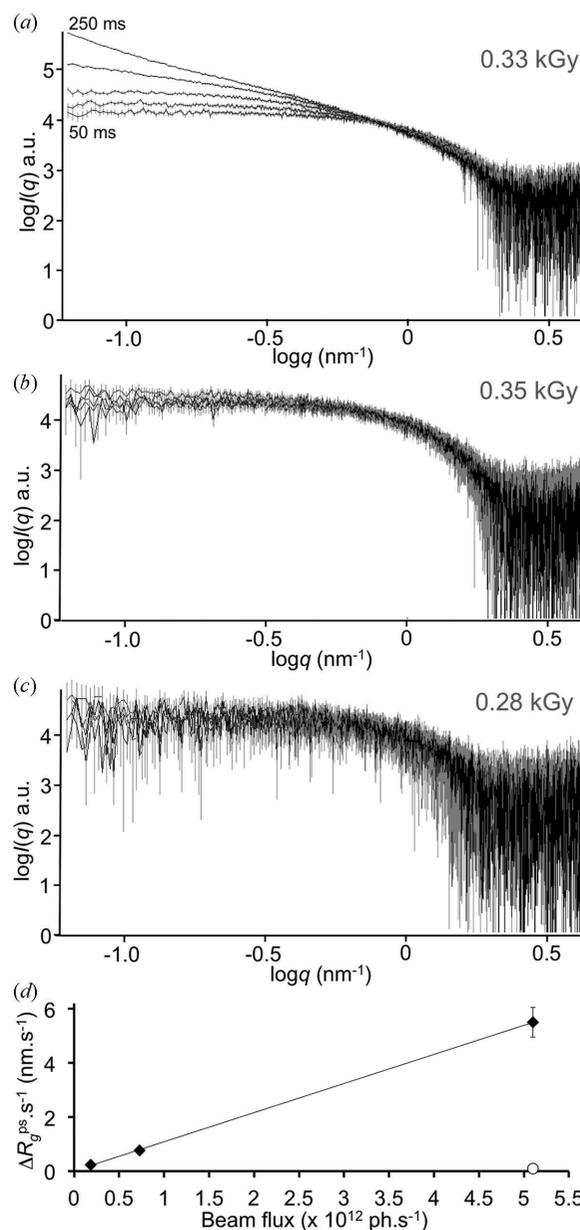
Figure 2
The effects of beam attenuation. SAXS data (5 × 50 ms exposures) recorded from static 4.4 mg ml^{-1} lysozyme samples collected at: (a) 5.1×10^{12} photons s^{-1}, (b) 7.3×10^{11} photons s^{-1}, (c) 1.8×10^{11} photons s^{-1}. The critical dose, in kGy, for the lysozyme samples at each level of attenuation is reported on each plot. (d) The initial rates of damage (black diamonds) are compared with the initial rate of damage at full beam flux with sample flow enabled (white circle). Initial rates were estimated from static samples exposed to approximately the same dose per frame by adjusting the exposure time at each level of attenuation (50 ms, 0.32 s and 1.41 s, for no, medium and high attenuation, respectively).

not the absolute value of the dose that is important but rather the number of SAXS data frames that can be collected from undamaged samples up to the critical dose time and what steps can be taken to increase this safe collection time either *via* beam attenuation or by modifying the solvent conditions (see below). Complicating matters, the critical dose is likely to change with solvent conditions (salt, pH, *etc*), which may (or may not) cause a shift in protein equilibrium towards states prone to either chemical or radiation-induced aggregation.

The main advantage afforded by beam attenuation is that there is no need to alter the sample conditions to reduce the effects of radiation damage. However, the benefits of attenuation must be assessed in terms of compromised scattering signal intensities and an overall reduction in the quality of the data. From Fig. 2(*c*) it can be seen that, as the beam is attenuated, the noise in the scattering signal increases. Therefore, the choice to attenuate the incident beam must be evaluated in terms of data quality *versus* sample quantity and by the type of SAXS experiment. For standard batch mode analysis it may be necessary to collect data from several aliquots of a highly sensitive sample with both beam attenuation and sample flow enabled in order to acquire sufficient frames to produce an averaged SAXS profile with reasonable counting statistics.

For continuous-flow SEC-SAXS experiments, attenuation may act to prevent the slow build-up of aggregates on the SAXS capillary as each component flows through the X-ray beam. Unlike batch-mode SAXS where the sample cell is cleaned between successive runs, there are no opportunities to wash the SAXS capillary while the different sample components elute from the separation column, and capillary fouling is often observed. Attenuation can thus reduce this build up of aggregates. On the other hand, the increased number of data frames (25–100 1 s frames measured for each component eluting from a SEC column) and their subsequent averaging can compensate for the decreased scattering intensities caused by the reduction in flux.

3.3. Solution additives

The effect of altering protein concentration of several different protein samples (BSA, GI, cytochrome C, lysozyme and RNAse) with respect to their initial rates of aggregation are shown in Fig. S2 of the supporting information. The addition of DTT, ascorbic acid and glycerol were assessed on their ability to reduce radiation damage (Kuwamoto *et al.*, 2004; Skou *et al.*, 2014; Grishaev, 2012; Jacques & Trewhella, 2010) in these samples using a full X-ray beam and no sample flow. Example scattering profiles obtained from RNAse at 10 mg ml^{-1} without and with additives present are shown in Fig. 3. All three additives reduce the production of aggregates, with 5% *v/v* glycerol being particularly effective in inhibiting radiation damage (ΔR_g^{ps} s$^{-1} \simeq 0.2$ nm s^{-1}). The RNAse data displayed in Fig. 3(*d*) (5 × 30 ms frames) are equivalent (*p* > 0.35) and radiation damage in the sample was first detected after 300 ms total exposure. A comparison between the radiation sensitivity of GI, BSA, cytochrome-C, lysozyme and
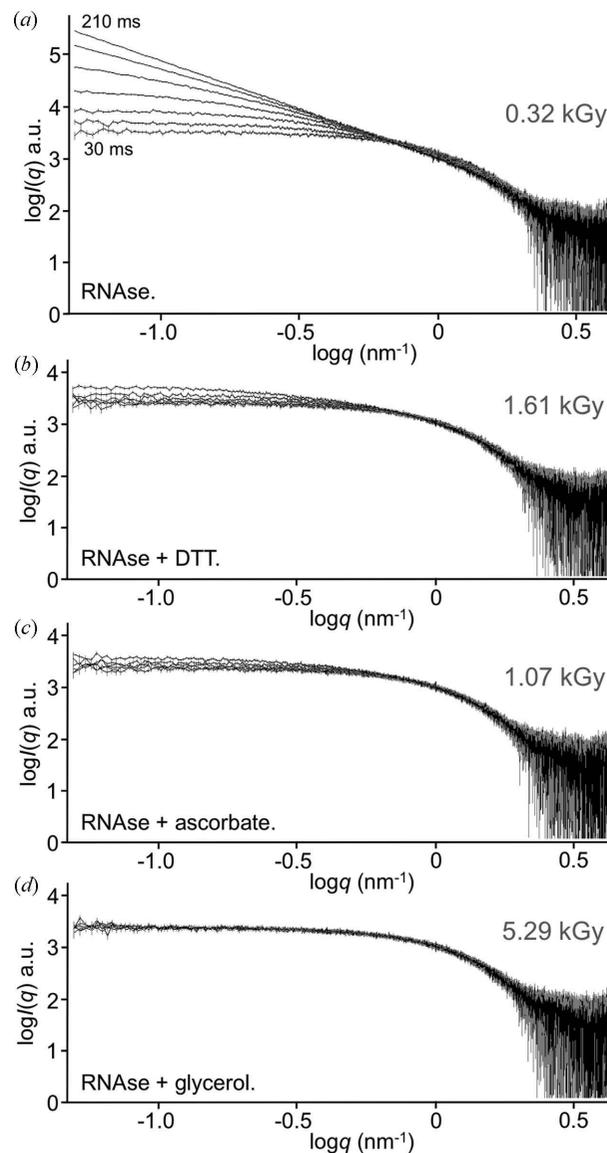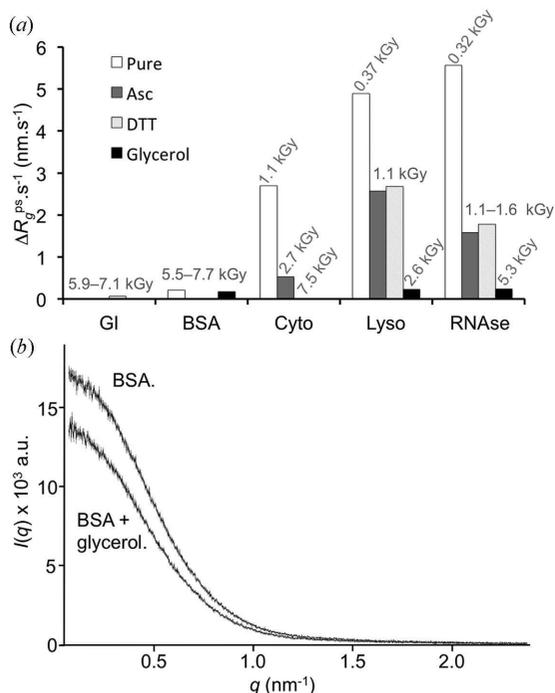
Figure 3
The effect of solution additives on limiting radiation damage: RNAse case study. (*a*) RNAse SAXS data (7 × 30 ms exposures; 10 mg ml^{-1}) collected at full flux with no sample flow show severe radiation damage after 30 ms exposure. The addition of 1 m*M* DTT (*b*), 1 m*M* ascorbate (*c*) and 5% *v/v* glycerol (*d*) significantly reduce radiation damage to the sample. In the case of glycerol, damage is not detected until after 300 ms exposure to the full beam. The critical dose (kGy) for RNAse under each condition is reported on each plot.

RNAse demonstrate that the initial rate of damage varies considerably, depending on the protein sample (Fig. 4*a*). In general, 1 m*M* DTT, 1 m*M* ascorbic acid and 5% *v/v* glycerol all contribute to reducing the initial rates of radiation damage in the different protein samples, although their effects are more apparent in those samples with initially high radiation sensitivity (*e.g.* lysozyme and RNAse).

The advantage of doping a sample with solution additives is that it is relatively straightforward for users to add these components to samples 'at the beamline'. However, for batch-mode sample delivery, care has to be taken when adding accurate and equal measures of additive to both the sample and to the corresponding solvent blank to ensure that a

Figure 4
Radiation susceptibilities of different proteins and the effect of solution additives. (a) Histogram comparing the initial rates of radiation damage calculated across 5×30 ms exposure frames for GI (10 mg ml^{-1}), BSA (11 mg ml^{-1}), cytochrome-C (Cyto, 10 mg ml^{-1}), lysozyme (Lyso, 8.8 mg ml^{-1}) and RNAse (10 mg ml^{-1}) with and without solution additives present (Asc, ascorbate, 1 mM; DTT, dithiothreitol, 1 mM; glycerol, 5% v/v; GI/glycerol and Cyto/glycerol measurements are not included). Estimates of the critical dose (kGy) are reported (for further details refer to Table S4 of the supporting information). (b) The effect of 5% v/v glycerol on the solvent-corrected SAXS scattering intensities of BSA in solution as a consequence of reducing X-ray contrast.

the final scattering profiles. As an example, in Fig. 4(b) the final scattering profiles for BSA at 11 mg ml^{-1} with or without 5% v/v glycerol in solution illustrate the $\sim$20% reduction in $I(q)$ across all of q as a consequence of glycerol addition. Therefore, although the addition of glycerol (or other types of polyol, e.g. sucrose) might be effective in counteracting radiation damage (Kuwamoto et al., 2004), these electron-dense materials can compromise signal intensities if added to samples in excess, or could influence protein–solvent/protein–proteins interactions (Vagenende et al., 2009) potentially altering oligomeric states. Based on the data presented here, the choice of up to 5% v/v glycerol appears to be a balanced compromise between maintaining reasonable contrast and significantly reducing the effects of radiation damage. It must also be noted that additive concentration screening may be required depending on the sensitivity of samples, necessitating increased sample volumes. Alternative small molecules to limit radiation damage suggested by Grishaev (2012) include tris(2-carboxyethyl)phosphine (TCEP; a more stable reducing agent), ethylene glycol and the use of tris or HEPES buffers.

4. Conclusions

Here simple practical strategies for limiting radiation damage that users of the BioSAXS P12 beamline can easily implement during the course of their allocated experiment have been described and compared. Flow measurements can be combined with a reduction in exposure time or beam attenuation to reduce the dose per unit volume of irradiated sample or the addition of small molecules to samples to help scavenge free radicals and/or stabilize protein constituents to
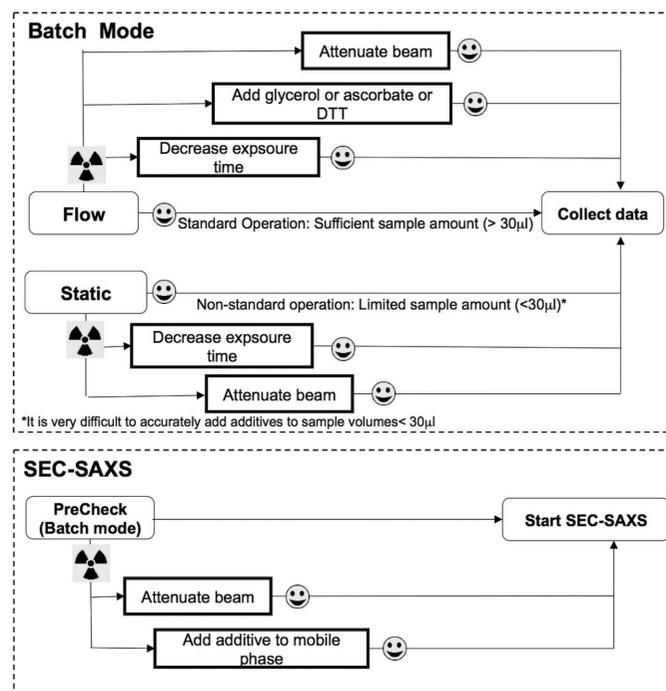
solvent mis-match does not occur (Jacques & Trewhella, 2010). If time is limited, well calibrated pipettes or a microbalance can be used to add an equal volume or mass of concentrated additive stock solutions, although extreme care has to be applied when handling viscous glycerol solutions. If a user has additional time and is not sample-limited, dialysis is preferable. For SEC-SAXS, the pressure limit on the column for the experiment has to be considered when using glycerol in the mobile phase. The sepharose-based analytical columns employed at P12 for SEC-SAXS experiments can withstand 5% v/v glycerol without damaging the column matrix.

The major disadvantage of the solution additive approach is that the chemical environment of the sample will change which increases the risk of altering the chemical or physical properties of a protein. For example, the addition of DTT to a protein that is otherwise maintained in an oxidized state might reduce disulfide bonds resulting in undesirable changes in structure. DTT also undergoes oxidation that changes its ultraviolet (280 nm) absorption properties that may affect protein concentration estimates (Grishaev, 2012; Jacques & Trewhella, 2010). Glycerol, on the other hand, alters the contrast of a sample. The difference in scattering length or electron density between the protein and solvent is reduced on glycerol addition that diminishes the scattering intensities in

Figure 5
General SAXS data collection scheme for users of the EMBL P12 BioSAXS beamline, PETRAIII.

ultimately reduce the rate and extent of aggregation. The effect of these small molecules, in particular glycerol, is to limit radiation damage, although their addition to the solution has to be considered on a case-by-case basis and in the context of maintaining the integrity of samples and the data quality. The general SAXS data collection scheme for users using the P12 beamline is summarized as a flow-chart in Fig. 5.

References

Berger, M. J., Hubbell, J. H., Seltzer, S. M., Chang, J., Coursey, J. S., Sukumar, R., Zucker, D. S. & Olsen, K. (2010). *XCOM: Photon Cross Section Database* (Version 1.5). National Institute of Standards and Technology, Gaithersburg, MD, USA. (Available Online: http://physics.nist.gov/xcom.)

Blanchet, C. E., Zozulya, A. V., Kikhney, A. G., Franke, D., Konarev, P. V., Shang, W., Klaering, R., Robrahn, B., Hermes, C., Cipriani, F., Svergun, D. I. & Roessle, M. (2012). *J. Appl. Cryst.* **45**, 489–495.

Fischetti, R. F., Rodi, D. J., Mirza, A., Irving, T. C., Kondrashkina, E. & Makowski, L. (2003). *J. Synchrotron Rad.* **10**, 398–404.

Franke, D., Kikhney, A. G. & Svergun, D. I. (2012). *Nucl. Instrum. Methods Phys. Res. A*, **689**, 52–59.

Garrison, W. M. (1987). *Chem. Rev.* **87**, 381–398.

Gasteiger, E., Hoogland, C., Gattiker, A., Duvaud, S., Wilkins, M. R., Appel, R. D. & Bairoch, A. (2005). *Protein Identification and Analysis Tools on the ExPASy Server*, in *The Proteomics Protocols Handbook*, edited by J. M. Walker, pp. 571–607. Totowa: Humana Press.

Graceffa, R., Nobrega, R. P., Barrea, R. A., Kathuria, S. V., Chakravarthy, S., Bilsel, O. & Irving, T. C. (2013). *J. Synchrotron Rad.* **20**, 820–825.

Grant, T. D., Luft, J. R., Wolfley, J. R., Tsuruta, H., Martel, A., Montelione, G. T. & Snell, E. H. (2011). *Biopolymers*, **95**, 517–530.

Grishaev, A. (2012). *Curr. Protoc. Protein. Sci.* **70**, 17.14.1–17.14.18.

Guinier, A. (1939). *Ann. Phys. (Paris)*, **12**, 161–237.

Henke, B. L., Gullikson, E. M. & Davis, J. C. (1993). *At. Data Nucl. Data Tables*, **54**, 181–342.

Hura, G. L., Menon, A. L., Hammel, M., Rambo, R. P., Poole, F. L. II, Tsutakawa, S. E., Jenney, F. E. Jr, Classen, S., Frankel, K. A., Hopkins, R. C., Yang, S., Scott, J. W., Dillard, B. D., Adams, M. W. W. & Tainer, J. A. (2009). *Nat. Methods*, **6**, 606–612.

Jacques, D. A. & Trewhella, J. (2010). *Protein Sci.* **19**, 642–657.

Kuwamoto, S., Akiyama, S. & Fujisawa, T. (2004). *J. Synchrotron Rad.* **11**, 462–468.

Maleknia, S. D., Ralston, C. Y., Brenowitz, M. D., Downard, K. M. & Chance, M. R. (2001). *Anal. Biochem.* **289**, 103–115.

Martel, A., Liu, P., Weiss, T. M., Niebuhr, M. & Tsuruta, H. (2012). *J. Synchrotron Rad.* **19**, 431–434.

Mathew, E., Mirza, A. & Menhart, N. (2004). *J. Synchrotron Rad.* **11**, 314–318.

Meisburger, S. P., Warkentin, M., Chen, H. M., Hopkins, J. B., Gillilan, R. E., Pollack, L. & Thorne, R. E. (2013). *Biophys. J.* **104**, 227–236.

Mylonas, E. & Svergun, D. I. (2007). *J. Appl. Cryst.* **40**, s245–s249.

Nielsen, S. S., Møller, M. & Gillilan, R. E. (2012). *J. Appl. Cryst.* **45**, 213–223.

Pernot, P., Theveneau, P., Giraud, T., Fernandes, R. N., Nurizzo, D., Spruce, D., Surr, J., McSweeney, S., Round, A., Felisaz, F., Foedinger, L., Gobbo, A., Huet, J., Villard, C. & Cipriani, F. (2010). *J. Phys. Conf. Ser.* **247**, 012009.

Petoukhov, M. V., Franke, D., Shkumatov, A. V., Tria, G., Kikhney, A. G., Gajda, M., Gorba, C., Mertens, H. D. T., Konarev, P. V. & Svergun, D. I. (2012). *J. Appl. Cryst.* **45**, 342–350.

Petoukhov, M. V., Konarev, P. V., Kikhney, A. G. & Svergun, D. I. (2007). *J. Appl. Cryst.* **40**, s223–s228.

Skou, S., Gillilan, R. E. & Ando, N. (2014). *Nat. Protoc.* **9**, 1727–1739.

Vagenende, V., Yap, M. G. S. & Trout, B. L. (2009). *Biochemistry*, **48**, 11084–11096.

Whitten, A. E., Cai, S. & Trewhella, J. (2008). *J. Appl. Cryst.* **41**, 222–226.